

3D printing-based mirrored image component for seamless modular curved-edge displays

SEUNGHWAN LEE,^{1,2} CHANHYUNG YOO,¹ HYUNGSOO YOON,^{1,2}
DONGYEON KIM,¹ GEONHEE KIM,^{1,2} BYOUNGHO LEE,^{1,2} AND
YONGTAEK HONG^{1,2,*} 

¹Department of Electrical and Computer Engineering, Seoul National University, 1 Gwanak-ro, Gwanak-gu, Seoul 08826, Republic of Korea

²Inter-University Semiconductor Research Center (ISRC), Seoul National University, 1 Gwanak-ro,

Gwanak-gu, Seoul 08826, Republic of Korea

*yongtaek@snu.ac.kr

Abstract: A facile method for designing and fabricating a concave mirror from a 3D printed mold is proposed for a seamless modular curved-edge display. The concave mirror is placed on the seam of modular curved-edge display, thereby reflecting images at the curved-edge area toward the observer direction. By investigating the concave mirror structures based on parametric modeling, we obtain a continuous image in a modular curved-edge display by optically concealing the seam. We also analyze the luminance distribution and the viewing angle of the seamless modular curved-edge display to show the capability of concealing the seam by the concave mirror.

© 2021 Optical Society of America under the terms of the [OSA Open Access Publishing Agreement](#)

1. Introduction

The tiling of multiscreens is one of the key enabling technologies for large-area display applications through the arrangement of panels in the same plane. Due to the high cost and low production yield of large-area displays, this approach has been widely adopted in the display industry [1]. Furthermore, the tiling method is suitable for simply implementing modular displays by customizing the arrangement of panels according to the place, the size of the space, and personal preferences. However, the mechanical frame around the panel, which is called the seam, prevents observers from watching a continuous image through modular displays. Several methods have been suggested to demonstrate seamless modular images, including overlapping the seam [2], reducing the width of the seam [3], and attaching additional optical components onto the seam for optical cloaking [4–6]. Overlapping the seam is advantageous in that it only overlaps the edges of panels, but it has the disadvantage of increasing the thickness of the overall screen and requiring complex mechanical design for precise alignment of each panel. The second method is an approach to reduce the area of the gate driver region, but it is almost impossible to completely remove the seam due to the physical limitations of fining and redesigning the circuit system.

The planoconvex lens is a representative example of an optical component that can be applied to the seam [4]. By attaching the lens onto the seam directly, the image from the vicinity of the seam is expanded toward the seam, thereby optically concealing the seam and showing a continuous image. Despite the simple fabrication process with dispensing transparent optical adhesive onto the seam directly in this approach, a narrow viewing angle has been a bottleneck due to the limited available range of the virtual image expanded by the lens. As an alternative to the refractive optical component, a waveguide can act as a transformation element of edge and corner images, thereby developing a zero-seam flat panel display module [5,6]. This study shows a wide range of viewing angles, but it is difficult to apply to large-area displays due to the high cost of waveguides.

The seamless modular display technologies described so far have been applied only in flat panel displays. Displays with diverse form factors are required to provide a new user experience to the

consumer. Curved-edge displays with flexible panels have been widely used in commercialized products for their widescreen view and aesthetic benefits due to the curvature of the edge [7]. In addition to large displays, small- to medium-sized displays such as smartphones and tablet computers can be tiled to form modular displays. It is possible to utilize curved-edge display panels as a part of a modular display because the seam of curved-edge displays is narrow [8]. However, the modular image is still seen discontinuously. Therefore, seam concealment methods for curved-edge displays should be developed for the new form factors of modular displays. Utilization of a concave mirror, which has been used in various projection-type optical systems, including three-dimensional (3D) displays [9], panoramic imaging [10], and laser beam scanners [11], is considered as an option for demonstrating seamless modular curved-edge displays.

There is a need for a technique that makes it easier to fabricate large-scale optical components for seamless modular display applications. Although additive manufacturing has been employed as a cost-effective method, including dispensing [12] and screen printing [13], it is challenging to control the desired shape with such methods. To solve this problem, 3D printing, such as fused deposition modeling (FDM) [14] and stereolithography (SLA) [15], has been adopted in various fields for the rapid production of mechanical components [16] and electric circuits [17]. Optical components can also be quickly fabricated as designed using 3D printing and thereby utilized as prototypes. However, although there have been several reports about the fabrication and evaluation of 3D printed optical components such as lenses [18], prisms [19], and mirrors [20], there are few practical applications. For this reason, attempts to expand the applications of 3D printed optical components have been ongoing, especially in display and imaging devices [21,22]. Furthermore, molded optics are being employed in 3D printing for repeatable production of prototypes and parts that are difficult to fabricate by direct printing [23].

Based on the background mentioned above, we propose a method for designing and fabricating a concave mirror as an optical component from a 3D printed mold for seamless modular curved-edge display applications. Figure 1(a) shows a tiling of two curved-edge displays. The concave mirror is placed between the curved-edge displays, concealing the seam and showing an overall continuous image by reflecting the image at the curved-edge area toward the observer direction, as shown in Fig. 1(b). By investigating how the structure of the concave mirror affects the appearance of seamlessness according to geometric optics and parametric modeling based on the configuration of the curved-edge display system, image discontinuity between the curved-edge displays is shown to be mitigated. We also measure and analyze the luminance distribution and the viewing angle of the seamless modular curved-edge display to verify the seam concealment

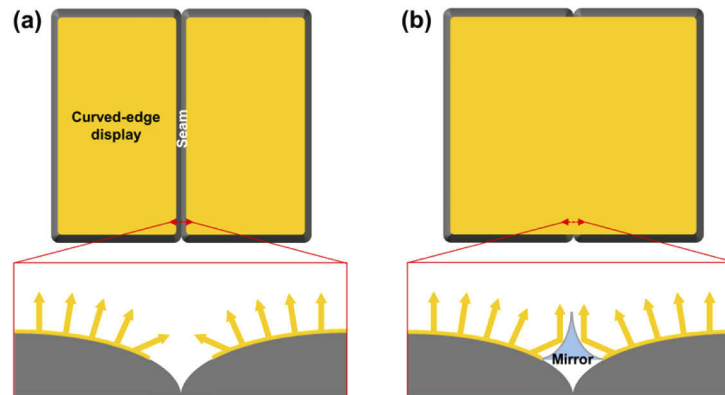


Fig. 1. Schematic diagram of modular curved-edge display (a) without and (b) with a concave mirror. The insets show cross-sectional images of the displays.

effect by the concave mirror. Finally, we suggest the possibility of reducing image distortion caused by the concave mirror and refer to the realization of various forms of screen devices through the seamless modular curved-edge displays as future works.

2. Experimental section

2.1. Design and fabrication of a concave mirror

For parametric curve modeling of the cross-sectional profile of the concave mirror, the rational Bézire conic curve is adopted, which is widely used in computer-aided design (CAD) [24]. The reason why the rational Bézire curve is selected is that the shape of the concave mirrors can be defined only with the height, width, and weight value. The stereolithography (STL) file of the designed concave mirror mold is generated with CAD software (Fusion 360, Autodesk) and transferred to an FDM-type 3D printer (DP200, Sindoh). A polylactic acid (PLA) plastic mold with 100 μm resolution (thickness of 1 layer) is fabricated and firmly attached to a glass substrate with an acrylic foam tape (VHBTM tape, 3M) to prevent mechanical deformation from thermal expansion during the thermal curing process of polydimethylsiloxane (PDMS). The PDMS base and curing agent (Sylgard 184, Dow Corning) are mixed at a weight ratio of 10:1 by a centrifugal paste mixer (ARE-310, Thinky) and poured into a concave mirror mold. Air bubbles that are generated during pouring are removed in a vacuum desiccator for approximately 1 hour. After thermal curing at 120 °C for 30 min, the PDMS replica is detached from the concave mirror mold. For surface planarization of the PDMS replica, a mixture of the PDMS base and curing agent with the same weight ratio as the PDMS replica is coated by spin coater (SPIN-1200D, Midas System) at 1200 rpm for 60 s. After that, the surface planarized PDMS replica is thermally cured again at 120 °C of 30 min and then treated with ultraviolet (UV) cleaner (AH-1700, Ahtech LTS) at 184 nm/254 nm wavelength and 30 mW cm^{-2} intensity for 30 min to form a silica-like layer on the PDMS surface. Finally, an aluminum (Al) layer of 50 nm thickness is deposited with a customized vacuum thermal evaporator (Woosung Hi-vac) under 10^{-5} torr, thereby completing the fabrication of the concave mirror.

2.2. Characterizations and measurements of mirror layer and seamless modular curved-edge display

The total reflectance (R_T) and diffuse reflectance (R_D) of the Al layer are measured by a spectrophotometer (CM-5, Konica Minolta) in the range from 360 nm to 740 nm with a 10 nm interval. The specular reflectance (R_S) is calculated by subtracting R_D from R_T . The cross-sectional views of PDMS replicas are observed with an optical microscope (OM) (DSX510, Olympus) in bright field mode. The surface morphology images of the Al layer in the top view are captured with a field emission scanning electron microscope (SEM) (S-4800, Hitachi). The surface roughness of the Al layer is measured by atomic force microscope (AFM) (XE-100, Park System) in noncontact mode. The luminance distribution is analyzed with ray-tracing simulation software (LightTools 8.5, Synopsys) and measured along the modular curved-edge display under the white image in the horizontal direction by using a luminance meter (CS-200, Konica Minolta) at a distance of 500 mm and an aperture of 0.1°. The pixels of the curved-edge display and their reflected images by the concave mirror are captured with an OM (DSX510, Olympus) in dark field mode. A Galaxy Note Edge (SM-N915S, Samsung Electronics) is selected as a curved-edge display product to demonstrate the seamless modular display.

3. Results and discussion

3.1. Design of a concave mirror

Figure 2(a) represents an imaging system involving a concave mirror in a seamless modular curved-edge display. The projection image generated by the reflection of the image at the

curved-edge area from the concave mirror should be inverted so that observers can see the continuous image from the front view. The reflected image covers the seam, thereby leading to an optical seam concealment effect. Although the emitted light from the pixels of the curved-edge display diverges, only the reflected light toward the observer is expressed in Fig. 2(a). In general, the concave mirrors are capable of optically forming images in midair [25], and the observer recognizes this image in the projected form. This is the reason for representing the reflected images as a projection type and the reflected light in parallel to the observed direction.

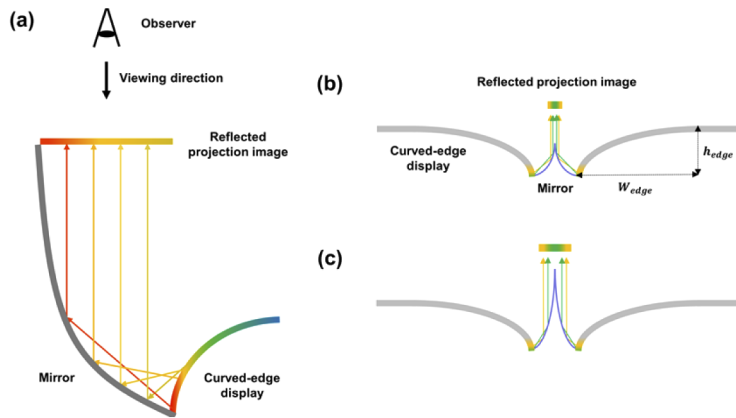


Fig. 2. (a) Principle of seamlessness in curved-edge modular displays with a reflected projection image generated by a concave mirror. Comparison of the light path from the image near the boundary of the curved-edge display and concave mirror when showing reflected projection images with (b) small and (c) large sizes according to the concave mirror structure. The emission point and direction of the ray are assumed to be the same for (b) and (c).

To find the concave mirror structure that displays a continuous image in the modular curved-edge display, a concave mirror with a width of 5.14 mm is placed on the seam formed by attaching two commercialized curved-edge display panels. Figure 2(b) and 2(c) show a comparison of the light path according to the concave mirror structure. In Fig. 2(b), the reflective projection image cannot cover the area near the boundary of the curved-edge display and the concave mirror. As a result, the seam is still observed in front of the modular curved-edge display. Therefore, it is necessary to find a concave mirror structure to expand the reflective projection image to enhance the seam concealment effect, as shown in Fig. 2(c). The reason for reflective projection image expansion with the increasing of the height of the concave mirror is that the reflected area on the concave mirror surface increases. The curved-edge display used in the experiment has an edge width (W_{edge}) of 7.03 mm and an edge height (h_{edge}) of 3.05 mm, and the edge curve is fitted with a parabola.

3.2. Fabrication process of a concave mirror with a 3D printed mold

Figure 3(a) shows the fabrication process of a concave mirror with a 3D printed mold. First, the concave mirror mold is fabricated by 3D printing with the FDM method, which uses thermoplastic material as a filament [14]. PLA is selected as a printing material for concave mirror molds and is the most widely commercialized materials in the 3D printing industry due to its eco-friendliness and low-cost characteristics [26]. After that, PDMS liquid mixed with curing agent is poured into the mold and thermally cured. PDMS is selected because it is easy to be separated from the PLA mold [27], so the desired structure can be replicated well. The cured PDMS replica is detached from the concave mirror mold, followed by surface planarization with spin coating

of additional PDMS liquid and thermal curing. After treating the smooth surface of the PDMS replica with UV light, the Al layer, which acts as a mirror, is deposited by thermal evaporation. As a result, the fabrication of the concave mirror is completed.

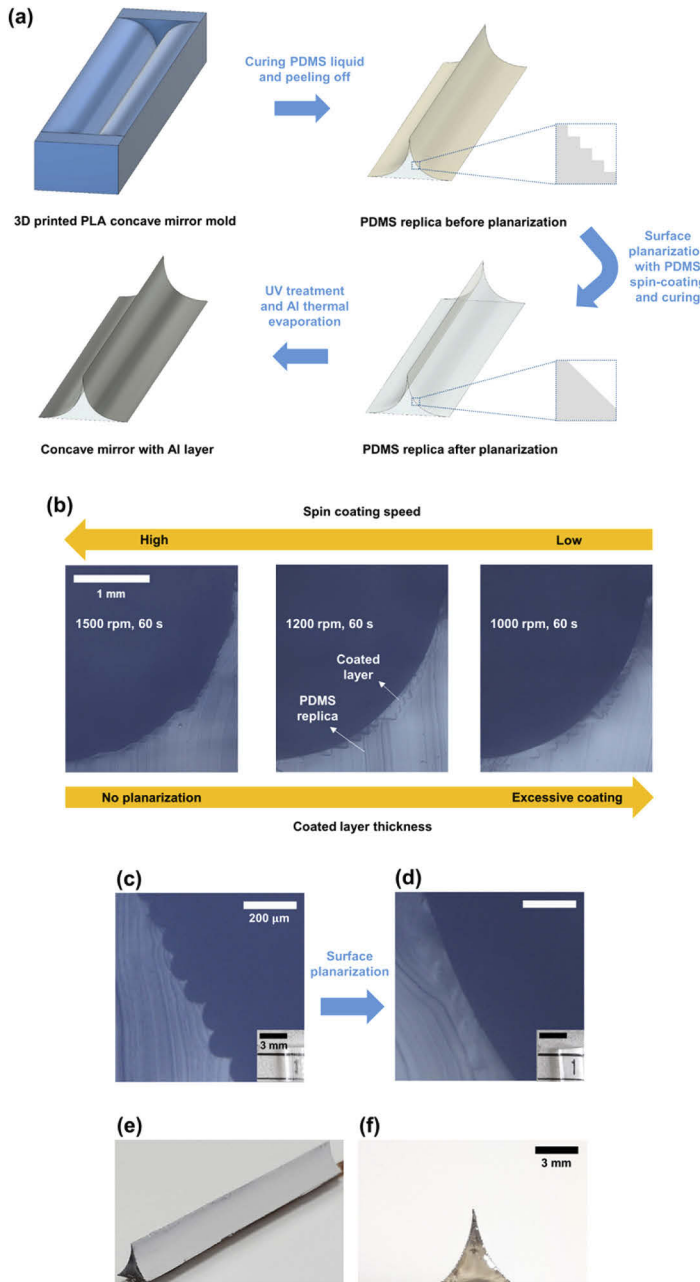


Fig. 3. (a) Fabrication process of a concave mirror with a 3D printed mold. The insets show cross-sectional images of PDMS replicas before and after surface planarization. (b) Relationship between spin coating speed and coated layer thickness of additional PDMS liquid. Images from the cross-sectional view of the PDMS replica (c) before and (d) after surface planarization. The insets show the PDMS replica on the number '1'. Camera images of the concave mirror from the (e) oblique and (f) cross-sectional view.

In general, surface planarization is conducted to fabricate optical components with 3D printing because their surface roughness should be on the order of tens of nm, which is much lower than that of a typical 3D printed structure with a scale of tens of μm . Methods for surface planarization have been developed, such as femtosecond laser smoothing [28] and meniscus equilibrium process [29]. However, femtosecond laser equipment is expensive, and it is difficult to precisely control the experimental conditions in meniscus equilibrium process. Unlike these two processes, spin coating of additional viscous liquid has the advantage of enabling surface planarization by merely adjusting the coating speed and time. Depending on the spin coating speed, the thickness of the coated layer varies, as shown in Fig. 3(b). It can be confirmed that surface planarization is completed under a certain spin coating speed. In Fig. 3(c) and 3(d), cross-sectional views of the PDMS replica before and after surface planarization are shown with OM. Before surface planarization, the surface of the PDMS replica protrudes because the surface of the 3D printed PLA mold protrudes. By spin coating additional PDMS liquid, the surface of the PDMS replica is flattened. The insets are the PDMS replica before and after surface planarization on the number ‘1’. Before surface planarization, the number appears blurry. However, it is clearly visible after surface planarization, indicating that the surface of the PDMS replica has been flattened. Figure 3(e) and 3(f) show the oblique and cross-sectional views of the fabricated concave mirror, respectively. The Al layer shows noticeably reflected surface without perceptible lines of 3D printed structure due to the smooth surface of the PDMS replica, thereby functioning as a mirror with a high specular reflection.

3.3. Reflectance and surface morphology of mirror layers

For the reflectance and the surface roughness measurements, flat samples of the mirror layers are prepared. Although the surface of the actual mirror layer is a curved shape, it is reasonable to measure a flat sample because the curved surface can be approximated like a plane in μm scale and a smooth surface can be obtained through the surface planarization even on a curved surface of 3D printed structure [30].

The R_T and R_D of the Al layers deposited on glass, bare PDMS, and UV-treated PDMS substrates are presented in Fig. 4(a) and 4(b). The reason for measuring the R_D is to determine the clarity of the reflected image. Generally, the R_D increases as the surface roughness increases [31]. When the metal layer is fabricated by thermal evaporation directly on the PDMS without any surface treatment, a wrinkled structure is formed due to thermal expansion of the PDMS surface by local heating and cooling to room temperature after finishing the process [32]. As a result, diffuse reflection occurs, showing a hazy reflected image. However, when UV treatment is applied to the PDMS surface, the thermal expansion of the PDMS is reduced due to the rigidity of the silica-like layer formed by UV light [33], thereby suppressing the formation of wrinkles. The surface roughness of the UV-treated PDMS surface is lowered so that a clear reflected image can be observed with the well-formed mirror layer. In the case of the glass, the Al layer exhibits an R_T of 91.97%, R_S of 90.99%, and R_D of 0.98% at a 550 nm wavelength. The Al layer on bare PDMS has an R_T of 23.89%, R_S of 1.06%, and R_D of 22.83% at the same wavelength. However, the Al layer on UV-treated PDMS shows an R_T of 91.87%, R_S of 90.84%, and R_D of 1.03%, comparable to the Al layer results for glass. In general, a reflected image without visual loss is observed when R_S is higher than 80% [34]. This means that the Al layer on UV-treated PDMS can be used as a mirror in seamless modular display systems.

Figure 4(c)–4(e) show the surface morphology of the Al layer on glass, bare PDMS, and UV-treated PDMS, respectively. In the top view of the SEM images, randomly formed wrinkles are observed in the Al layer on bare PDMS (Fig. 4(d)), while there are no wrinkles in the Al layer on glass (Fig. 4(c)) and UV-treated PDMS (Fig. 4(e)). The surface roughness of each sample is also examined by AFM measurement. Typically, the appropriate surface roughness range for optical components is lower than one-tenth of the visible light wavelength region (< 40

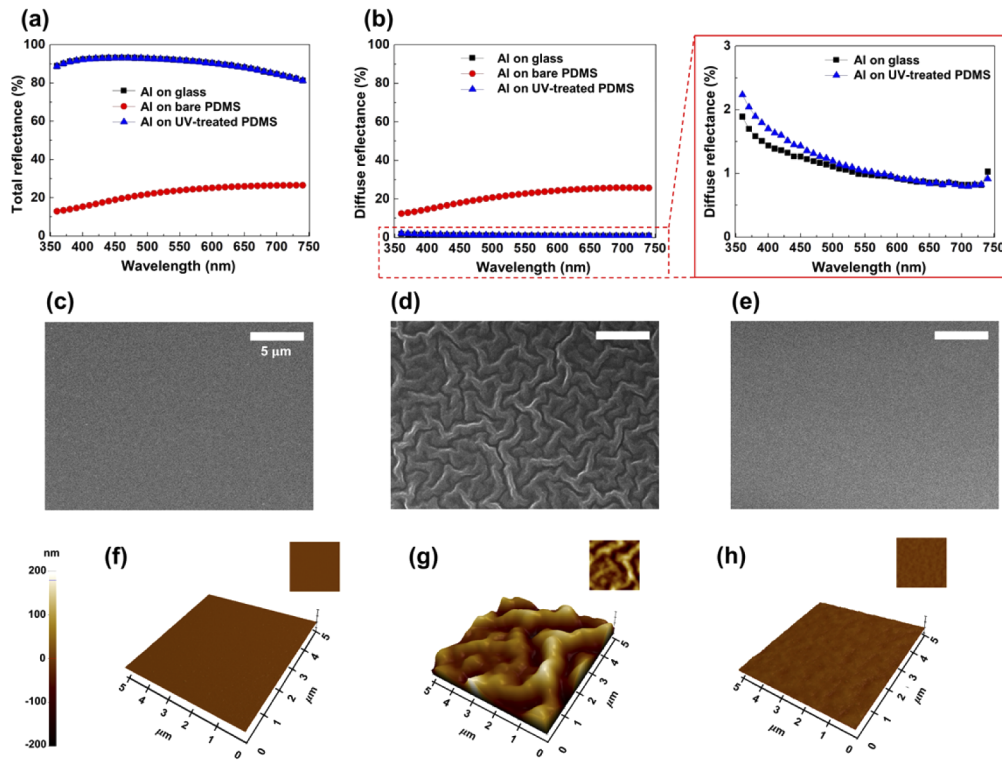


Fig. 4. (a) Total reflectance and (b) diffuse reflectance of the Al layer on glass, bare PDMS, and UV-treated PDMS. SEM images of the Al layer on (c) glass, (d) bare PDMS, and (e) UV-treated PDMS. AFM images of the Al layer on (f) glass, (g) bare PDMS, and (h) UV-treated PDMS.

nm) [35]. The surface roughness of the Al layer on bare PDMS is measured to be 63.782 nm root-mean-square (RMS) (Fig. 4(g)), while that of the Al layer on UV-treated PDMS decreases to 5.066 nm RMS (Fig. 4(h)), which is comparable to that of the Al layer on glass, with a value of 1.366 nm RMS (Fig. 4(f)). This indicates the suppression of wrinkles by UV treatment of the PDMS surface, and the Al layer on UV-treated PDMS satisfies the surface roughness requirement for utilization as a mirror.

3.4. Image continuity in the modular curved-edge display

To investigate the image continuity obtained with concave mirror structures, concave mirrors are fabricated by varying their structure parameters. Among them, four kinds of concave mirrors showing the change of the fill factor (FF) and the image continuity distinctly are selected, and their structural parameters are presented in Table 1. To quantify the image continuity, the FF is defined as the ratio of the reflected projection image area to the seam area from the front view. In Fig. 5(a), black lines are shown near the area where the curved-edge displays meet Mirror #1 because the mirror only reflects part of the light emitted from the images on the curved-edge displays, and the FF is 41.9%. Although the black lines are still observed in the case of both Mirror #2 and #3, portions of the reflected image on the seam area are increased to 48.4% and 58.1%, respectively. Finally, a seamless modular image is demonstrated with Mirror #4, and the widths of the black lines are reduced significantly, thereby representing an FF of approximately 100%. The oblique view of the seamless modular image is shown in Fig. 5(b) and a video file ([Visualization 1](#)).

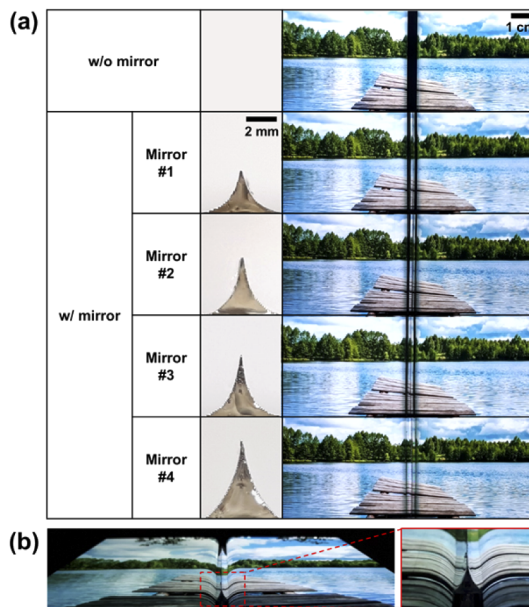


Fig. 5. (a) Variation in the image continuity of the modular curved-edge display according to the concave mirror structure. (b) Oblique view of the seamless modular image.

Table 1. Cross-sectional geometric parameters of concave mirrors for investigating image continuity of the modular curved-edge display. The weight is defined in [24].

Mirror	Width (mm)	Height (mm)	Type of rational Bézire curve	Weight
Mirror #1		2.80	Parabola	1.00
Mirror #2	5.14	3.82	Parabola	1.00
Mirror #3		4.13	Hyperbola	1.22
Mirror #4		5.22	Ellipse	0.67

3.5. Visual characteristics of seamless modular curved-edge display

After determining the concave mirror structure for the seamless modular curved-edge display, the luminance distributions of the modular images without and with the concave mirror are simulated and measured from the front view. According to previous studies related to seamless modular displays, the luminance distribution is the proper criterion to evaluate seamlessness [4]. Figure 6(a) shows the 3D optical modeling of the modular curved-edge display with the concave mirror for ray-tracing simulation, and the simulation results of the luminance distribution of the modular curved-edge display without and with the concave mirror are represented in Fig. 6(b) and 6(c). There is a difference in luminance in the seam area before and after placing the concave mirror, which means that the seam concealment effect is due to the concave mirror. At the position of $x = 0$, the average luminance in the seam area is increased from 3.23% to 60.63% in the simulation and from 4.62% to 74.85% according to measurement results by placing the concave mirror onto the seam, which verifies the seamlessness of the modular curved-edge display, as shown in Fig. 6(d). Since the luminance is measured from the front view, this result confirms that the luminance of the curved-edge display decreases as the slope of the edge increases. For enhancing the uniformity of the luminance distribution, it is possible to consider introducing prism [8] or cylindrical lens [36] structures. To observe the reflection area on the concave mirror in detail, the pixels of the curved-edge display and their reflected images by the concave mirror at

the h_{edge} are directly compared from the front view, as shown in Fig. 6(e) and 6(f). Although the reflected pixels by the concave mirror look hazy, their sizes are comparable to these of the curved-edge displays. It is confirmed that there is a small variation in the pixel size when viewed from the front.

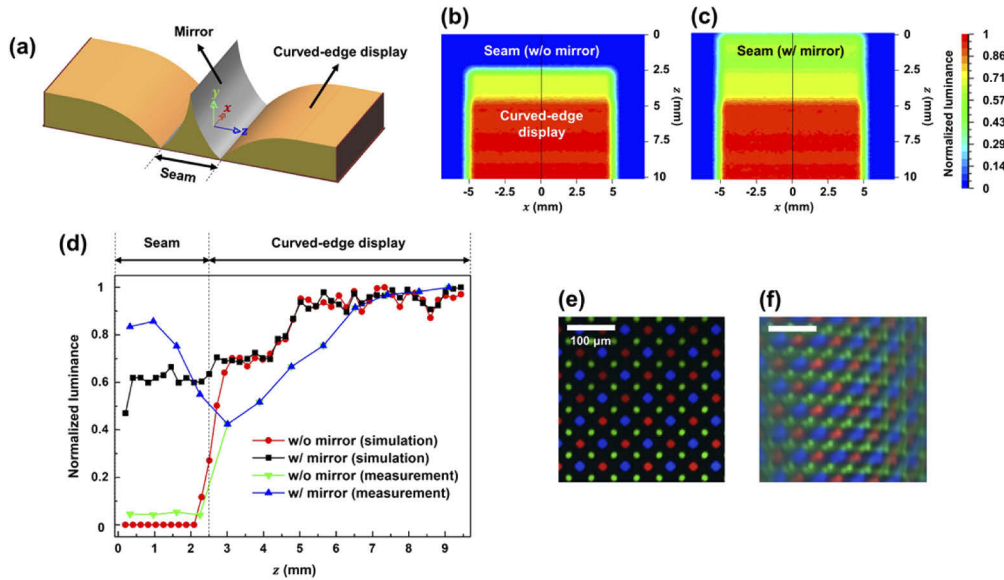


Fig. 6. (a) 3D optical modeling for ray-tracing simulation. Simulation results of the luminance distribution of a modular curved-edge display (b) without and (c) with a concave mirror. (d) Comparison of the luminance simulation and measurement results of a modular curved-edge display without and with a concave mirror at $x = 0$. (e) Pixels of a curved-edge display and (f) their reflected image by a concave mirror at the h_{edge} . The adopted concave mirror is Mirror #4.

The viewing angle of the seamless modular curved-edge display is also investigated. The viewing angle of a seamless modular display is defined as the maximum angular range at which the seam is not visible from the observer's view point. Although the reflected image becomes darker when the observation position is not the front (not on-axis), the seam is not visible in the viewing angle from -30° to $+30^\circ$ (rotation signs are defined in Fig. 7(a)), as shown in Fig. 7(b) and a video file ([Visualization 2](#)). It is presumed that the viewing range is limited because the areas that cannot be covered by the reflected image appear near the boundary of the concave mirror and the curved-edge display and the uncovered areas are enlarged from a certain viewing angle or more, thereby being observed as a black image.

Due to the limited resolution of 3D printers, the width of the concave mirror apex is the minimum feature length of a 3D printed structure, and its value is approximately $100 \mu\text{m}$, as shown in Fig. 8. According to previous research related to human vision, the angular resolution of a typical human eye is approximately 30 cycles per degree (cpd) [2]. If the angular resolution is converted to distance resolution, the viewing distance for resolving a length of $100 \mu\text{m}$ is calculated to be 344.8 mm . In general, the viewing distance of small- and medium-sized displays is approximately 300 mm [37]. Therefore, the concave mirror apex can be recognized by the observer because the viewing distance is shorter than 344.8 mm . It is expected that the concave mirror apex will be imperceptible for the observer if it has a narrow width obtained by using a high-resolution 3D printer with a scale of tens of μm . Another issue is that the apex can be fragile due to its pointed shape during the separation of the replica from the 3D printed mold.

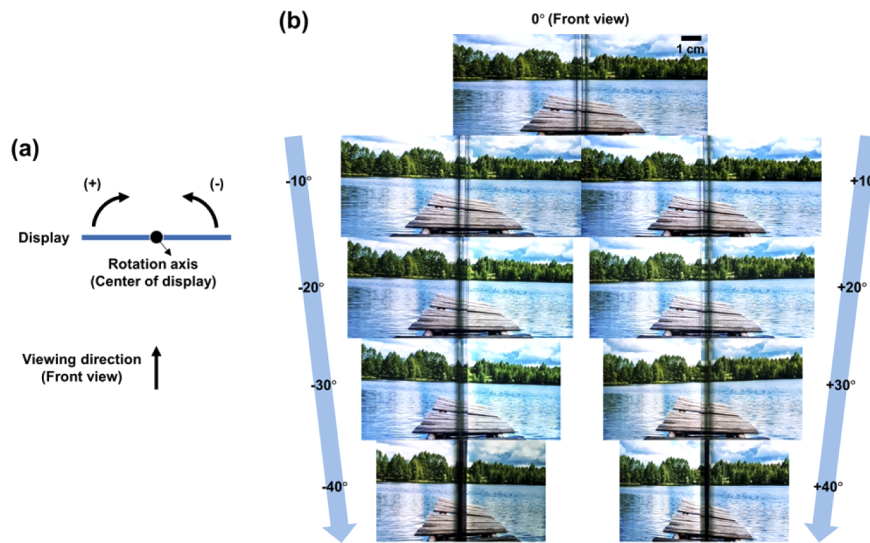


Fig. 7. (a) Definition of rotation signs. A positive sign (+) of the angle denotes clockwise rotation, and the opposite direction is represented as a negative sign (-) of the angle viewed from the front of the image. (b) Seamless modular curved-edge display from different viewing angles.

The width increases, and the shape changes if it is broken. As a result, it can affect the visual characteristics of the seamless modular curved-edge display such as the appearance of the black line. Therefore, it is necessary to consider the materials of replica and mold that can be well separated in the fabrication process of the concave mirror.

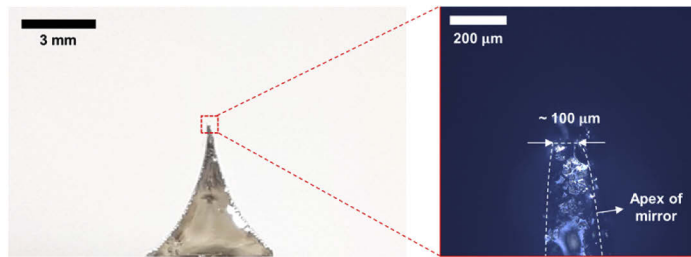


Fig. 8. Cross-sectional images of the concave mirror (Mirror #4) and its apex.

4. Conclusion

In summary, we have demonstrated a seamless modular curved-edge display with a concave mirror, which is designed and fabricated with a 3D printed mold. The concave mirror is placed on the seam of modular curved-edge displays to remove image discontinuity by reflecting the image at the curved-edge area toward the observer direction. By modifying the height and curvature of the concave mirror based on geometric optics and parametric modeling, we obtain a continuous image in a modular curved-edge display. We measure and analyze the luminance distribution and the viewing angle of a seamless modular curved-edge display to verify the seam concealment effect.

When implementing the seamless modular curved-edge display with a concave mirror, image distortion inevitably occurs due to the magnification of the original image. To alleviate the image distortion, a distortion correction technique can be utilized, which is a method for enhancing image quality in a head-mounted display [38]. This computational optics technique minimizes the difference between the target and the original image. Since the human eye cannot recognize individual pixels, distortion can be reduced by image processing in a way that increases the signal-to-noise ratio (SNR) of the overall image. It is expected that it is generally applicable to seamless modular curved-edge displays once the distortion correction is completed. Furthermore, a method of adjusting the curvature of the edge part as well as the concave mirror structure can be considered to improve the visual characteristics of the seamless modular curved-edge displays.

Through this work, we demonstrate the potential utilization of 3D printed optical components in the display industry. Furthermore, we expect that establishing a seamless modular display will pave the way for the realization of various forms of screen devices via a straightforward and cost-effective method.

Funding. Ministry of Trade, Industry and Energy (10051971).

Acknowledgments. This research was supported by the MOTIE (Ministry of Trade, Industry, & Energy) (10051971) and KDRC (Korea Display Research Corporation) support program for the development of future devices technology for display industry.

Disclosures. The authors declare no conflicts of interest.

References

1. A. C. Arias, J. D. MacKenzie, I. McCulloch, J. Rivnay, and A. Salleo, "Materials and applications for large area electronics: Solution-based approaches," *Chem. Rev.* **110**(1), 3–24 (2010).
2. M. Aston, "Design of large-area OLED displays utilizing seamless tiled components," *J. Soc. Inf. Disp.* **15**(8), 535–540 (2007).
3. K. M. Kim, I. Han, S. Noh, Y. I. Jang, K. Oh, B. Kim, and I. B. Kang, "Bezel free design of organic light emitting diode display via a-InGaZnO gate driver circuit integration within active array," *J. Soc. Inf. Disp.* **27**(8), 514–522 (2019).
4. S. Lee, S. Lee, H. Yoon, C. K. Lee, C. Yoo, J. Park, J. Byun, G. Kim, B. Lee, B. Lee, and Y. Hong, "Printed cylindrical lens pair for application to the seam concealment in tiled displays," *Opt. Express* **26**(2), 824–834 (2018).
5. S. Lee, J. Moon, S. Yang, J. Rhim, B. Kim, Y. Lee, S. Han, S. Yoon, and I. Kang, "Development of zero-bezel display utilizing a waveguide image transformation element," *Dig. Tech. Pap. - Soc. Inf. Disp. Int. Symp.* **48**(1), 612–614 (2017).
6. A. C. Lowe, P. A. Bayley, N. A. Gallen, M. Huang, and B. Needham, "A novel approach to tiled displays," *Dig. Tech. Pap. - Soc. Inf. Disp. Int. Symp.* **34**(1), 180–183 (2003).
7. V. C. Coffey, "The age of OLED displays," *Opt. Photonics News* **28**(11), 34–41 (2017).
8. K. D. Powell and J. M. Lutian, "Curved edge display with controlled luminance," *U.S patent 10,185,064B2* (22 January 2019).
9. J. Hong, Y. Kim, S. G. Park, J. H. Hong, S. W. Min, S. D. Lee, and B. Lee, "3D/2D convertible projection-type integral imaging using concave half mirror array," *Opt. Express* **18**(20), 20628–20637 (2010).
10. X. Wu, Y. Wu, and P. Wen, "Concave omnidirectional imaging device for cylindrical object based on catadioptric panoramic imaging," *Opt. Eng.* **57**(3), 033109 (2018).
11. Y. M. Sabry, D. Khalil, B. Saadany, and T. Bourouina, "Integrated wide-angle scanner based on translating a curved mirror of acylindrical shape," *Opt. Express* **21**(12), 13906–13916 (2013).
12. S. Ekgasit, N. Kaewmanee, P. Jangtawee, C. Thammacharoen, and M. Donphoongpri, "Elastomeric PDMS planoconvex lenses fabricated by a confined sessile drop technique," *ACS Appl. Mater. Interfaces* **8**(31), 20474–20482 (2016).
13. X. Zhou, Y. Peng, R. Peng, X. Zeng, Y. A. Zhang, and T. Guo, "Fabrication of large-scale microlens arrays based on screen printing for integral imaging 3D display," *ACS Appl. Mater. Interfaces* **8**(36), 24248–24255 (2016).
14. R. Melnikova, A. Ehrmann, and K. Finsterbusch, "3D printing of textile-based structures by fused deposition modelling (FDM) with different polymer materials," *IOP Conf. Ser.: Mater. Sci. Eng.* **62**, 012018 (2014).
15. X. Zhang, X. N. Jiang, and C. Sun, "Micro-stereolithography of polymeric and ceramic microstructures," *Sens. Actuators, A* **77**(2), 149–156 (1999).
16. T. Sathish, M. D. Vijayakumar, and A. K. Ayyangar, "Design and fabrication of industrial components using 3D printing," *Mater. Today: Proc.* **5**(6), 14489–14498 (2018).
17. G. T. Carranza, U. Robles, C. L. Valle, J. J. Gutierrez, and R. C. Rumpf, "Design and hybrid additive manufacturing of 3-D/volumetric electrical circuits," *IEEE Trans. Compon. Packaging Manuf. Technol.* **9**(6), 1176–1183 (2019).

18. G. D. Berglund and T. S. Tkaczyk, "Fabrication of optical components using a consumer-grade lithographic printer," *Opt. Express* **27**(21), 30405–30420 (2019).
19. S. S. Hinman, K. S. McKeating, and Q. Cheng, "Plasmonic sensing with 3D printed optics," *Anal. Chem.* **89**(23), 12626–12630 (2017).
20. N. Vaidya and O. Solgaard, "3D printed optics with nanometer scale surface roughness," *Microsyst. Nanoeng.* **4**(1), 18 (2018).
21. Y. L. Kong, I. A. Tamargo, H. Kim, B. N. Johnson, M. K. Gupta, T. W. Koh, H. A. Chin, D. A. Steingart, B. P. Rand, and M. C. McAlpine, "3D printed quantum dot light-emitting diodes," *Nano Lett.* **14**(12), 7017–7023 (2014).
22. K. Akşit, P. Chakravarthula, K. Rathinavel, Y. Jeong, R. Albert, H. Fuchs, and D. Luebke, "Manufacturing application-driven foveated near-eye displays," *IEEE Trans. Vis. Comput. Graph.* **25**(5), 1928–1939 (2019).
23. M. Schaub, J. Schwiegerling, E. C. Fest, A. Symmons, and R. H. Shepard, *Molded Optics: Design and Manufacture* (Taylor & Francis Group, 2011).
24. C. Blanc and C. Schlick, "Accurate parametrization of conics by NURBS," *IEEE Comput. Grap. Appl.* **16**(6), 64–71 (1996).
25. Y. Ishihara and M. Ishihara, "Correcting distorted objects formed in a concave mirror," in *Proceedings of ACM Symposium of User Interface Software and Technology*, paper 167 (2008).
26. X. Chen, G. Chen, G. Wang, P. Zhu, and C. Gao, "Recent progress on 3D-printed polylactic acid and its applications in bone repair," *Adv. Eng. Mater.* **22**(4), 1901065 (2020).
27. B. Kang, J. Sung, and H. So, "Realization of superhydrophobic surfaces based on three-dimensional printing technology," *Int. J. of Precis. Eng. and Manuf.-Green Tech.* **8**(1), 47–55 (2021).
28. X. Q. Liu, S. N. Yang, Y. L. Sun, L. Yu, B. F. Bai, Q. D. Chen, and H. B. Sun, "Ultra-smooth micro-optical components of various geometries," *Opt. Lett.* **44**(10), 2454–2457 (2019).
29. X. Chen, W. Liu, B. Dong, J. Lee, H. O. T. Ware, H. F. Zhang, and C. Sun, "High-speed 3D printing of millimeter-size customized aspheric imaging lenses with sub 7 nm surface roughness," *Adv. Mater.* **30**(18), 1705683 (2018).
30. Z. Hong and R. Liang, "IR-laser assisted additive freeform optical manufacturing," *Sci. Rep.* **7**(1), 7145 (2017).
31. H. E. Bennett and J. O. Porteus, "Relation between surface roughness and specular reflectance at normal incidence," *J. Opt. Soc. Am.* **51**(2), 123–129 (1961).
32. N. Bowden, S. Brittain, A. G. Evans, J. W. Hutchinson, and G. M. Whitesides, "Spontaneous formation of ordered structures in thin films of metals supported on an elastomeric polymer," *Nature* **393**(6681), 146–149 (1998).
33. K. Efimenko, W. E. Wallace, and J. Genzer, "Surface modification of sylgard-184 poly (dimethyl siloxane) networks by ultraviolet and ultraviolet/ozone treatment," *J. Colloid Interface Sci.* **254**(2), 306–315 (2002).
34. E. F. Barkman, "Specular and diffuse reflectance measurements of aluminum surfaces," *Appearance of Metallic Surfaces* **478**, 46–58 (1970).
35. S. A. Tsai, H. C. Wei, and G. D. J. Su, "Polydimethylsiloxane coating on an ionic polymer metallic composite for a tunable focusing mirror," *Appl. Opt.* **51**(35), 8315–8323 (2012).
36. X. C. Shan, T. Liu, M. Mohame, B. Salam, and Y. C. Liu, "Large format cylindrical lens films formed by roll-to-roll ultraviolet embossing and applications as diffusion films," *J. Micromech. Microeng.* **25**(3), 035029 (2015).
37. L. Spencer, M. Jakobsen, S. Shah, and G. Cairns, "Minimum required angular resolution of smartphone displays for the human visual system," *J. Soc. Inf. Disp.* **21**(8), 352–360 (2013).
38. N. Jiang, J. Chen, Y. Liu, and D. Weng, "Study on distortion correction of head-mounted displays based on hardware system," in *Proceedings of International Conference on Intelligent Science and Intelligent Data Engineering* (Springer, 2012), pp. 490–497.